



Ligustroflavone alleviates chronic kidney disease by inhibiting ferroptosis through the GSK3 β /NRF2 signaling pathway

Wen Zhang , Shaofan Wang , Yaru Wang , Sutianyi Li , Mingyue Chen , Jiayu Song & Yunwen Yang

To cite this article: Wen Zhang , Shaofan Wang , Yaru Wang , Sutianyi Li , Mingyue Chen , Jiayu Song & Yunwen Yang (2026) Ligustroflavone alleviates chronic kidney disease by inhibiting ferroptosis through the GSK3 β /NRF2 signaling pathway, Redox Report, 31:1, 2636421, DOI: 10.1080/13510002.2026.2636421

To link to this article: <https://doi.org/10.1080/13510002.2026.2636421>



© 2026 The Author(s). Published by Informa UK Limited, trading as Taylor & Francis Group



View supplementary material [↗](#)



Published online: 25 Feb 2026.



Submit your article to this journal [↗](#)



View related articles [↗](#)



View Crossmark data [↗](#)

Ligustroflavone alleviates chronic kidney disease by inhibiting ferroptosis through the GSK3 β /NRF2 signaling pathway

Wen Zhang^a, Shaofan Wang^b, Yaru Wang^c, Sutianyi Li^d, Mingyue Chen^e, Jiayu Song^f and Yunwen Yang^{id}^c

^aDepartment of Nephrology, Affiliated Hospital of Integrated Traditional Chinese and Western Medicine, Nanjing University of Chinese Medicine, Nanjing, People's Republic of China; ^bNational Clinical Research Center for kidney Diseases, Jinling Hospital, Nanjing, People's Republic of China; ^cNanjing Key Laboratory of Pediatrics, Children's Hospital of Nanjing Medical University, Nanjing, People's Republic of China; ^dMedical College, Yangzhou University, Yangzhou, People's Republic of China; ^eSchool of Health Management, Anhui Medical University, Hefei, People's Republic of China; ^fDepartment of Pediatric Nephrology, The Second Affiliated Hospital of Nanjing Medical University, Nanjing, People's Republic of China

ABSTRACT

Objectives: Chronic kidney disease (CKD) is a global public health concern, characterized by a gradual decline in kidney function, with death of renal tubular epithelial cells (RTECs) as a key pathological mechanism. This study investigated the protective effect of ligustroflavone in CKD and its potential molecular mechanisms.

Methods: *In vivo*, the unilateral ureteral obstruction (UUO) and folic acid-induced nephropathy (FAN) mouse models were employed to assess the effects of ligustroflavone. *In vitro*, RTECs were treated with erastin. Western blotting, qRT-PCR, immunofluorescence (IF), and immunohistochemistry (IHC) were performed to detect renal tubular injury both *in vivo* and *in vitro*.

Results: *In vivo*, ligustroflavone treatment significantly improved renal tubular damage and interstitial fibrosis in mice. Furthermore, our results demonstrated that ligustroflavone alleviated ferroptosis of RTECs by inhibiting GSK3 β activity and reducing lipid peroxidation in mice. *In vitro*, ligustroflavone treatment inhibited erastin-induced ferroptosis in RTECs. In addition, ligustroflavone inhibited activation of myofibroblasts induced by ferroptosis of RTECs. Mechanistically, ligustroflavone exerted its protect effects through the GSK3 β /NRF2 pathway by inhibiting GSK3 β and activating NRF2, thereby promoting GPX4 expression and suppressing ferroptosis.

Conclusions: In summary, ligustroflavone inhibits ferroptosis in RTECs and confers protection in CKD. These findings suggest that ligustroflavone holds promise as a potential therapeutic agent for CKD.

KEYWORDS

Ligustroflavone; CKD; GSK3 β ; NRF2; GPX4; fibrosis; antioxidant; ferroptosis

Background

Chronic kidney disease (CKD) affects at least 10% of the global population. It is characterized by a gradual decline in kidney function that eventually progresses to uremia and is associated with an increased risk of cardiovascular disease [1,2]. Between 1990 and 2017, the global prevalence of CKD rose by 29.3%, while the number of patients receiving dialysis increased by 43.1% and kidney transplants rose by 10.7% [3]. With the rising incidence and mortality rates, treatment costs for CKD patients continue to grow, thereby intensifying the socioeconomic burden. Consequently, there is an urgent need to slow CKD progression and to identify potential therapeutic targets [4]. Fibrosis is a hallmark of CKD and contributes to pathological changes in renal tissue, of renal cells, and inflammatory cell infiltration, ultimately resulting in loss of renal function. Injury and death of RTEC play a central role in CKD progression. Several repair mechanisms, including transformation and dedifferentiation, can trigger the conversion of TEC into mesenchymal cells [5].

CONTACT Yunwen Yang  yangyunwen@njmu.edu.cn  Nanjing Key Laboratory of Pediatrics, Children's Hospital of Nanjing Medical University, 72 Guangzhou Road, Nanjing 210008, People's Republic of China; Jiayu Song  songjiayu@njmu.edu.cn  Department of Pediatric Nephrology, The Second Affiliated Hospital of Nanjing Medical University, Nanjing, Jiangsu 210003, People's Republic of China
 Supplemental data for this article can be accessed online at <https://doi.org/10.1080/13510002.2026.2636421>.

© 2026 The Author(s). Published by Informa UK Limited, trading as Taylor & Francis Group
This is an Open Access article distributed under the terms of the Creative Commons Attribution-NonCommercial License (<http://creativecommons.org/licenses/by-nc/4.0/>), which permits unrestricted non-commercial use, distribution, and reproduction in any medium, provided the original work is properly cited. The terms on which this article has been published allow the posting of the Accepted Manuscript in a repository by the author(s) or with their consent.

There is growing evidence that ferroptosis, a form of programmed cell death driven by iron-dependent lipid peroxidation, is associated with renal tubular degeneration [6–8]. Consequently, ferroptosis has become a major research focus. In RTECs, ferroptosis is linked to mitochondrial dysfunction, excessive accumulation of reactive oxygen species (ROS) [9], and depletion of glutathione (GSH), making it a promising target for CKD intervention. Studies have demonstrated that in a CKD mouse model with 5/6 nephrectomy, cisplatin exacerbates kidney injury by inducing ferroptosis, whereas the ferroptosis inhibitor deferoxamine (DFO) exhibits anti-fibrotic effects [10]. In RTECs, ferroptosis can be triggered by environmental stressors such as ischemia-reperfusion and toxins, which disrupt the oxidant–antioxidant balance and lead to a lethal accumulation of lipid ROS [11,12]. Nuclear factor erythroid 2-related factor 2 (NRF2) exerts antioxidant effects by inhibiting lipid-derived reactive oxygen species through multiple pathways. Activation of NRF2 has been reported to inhibit ferroptosis in RTECs [13]. NRF2 induces the synthesis of glutathione synthase and upregulates antioxidant enzymes such as heme oxygenase-1 (HO-1) and NAD (P) H quinone dehydrogenase 1 [NQO1], thereby eliminating ROS and maintaining redox balance [12,14]. Glycogen synthase kinase 3 β (GSK-3 β) is a serine/threonine kinase that participates in numerous key cellular signaling pathways and regulates essential biological processes [15]. GSK3 β has been shown to play a critical role in neurodegenerative diseases [16,17]. A key feature of these disorders is that GSK3 β participates in cellular responses to oxidative stress, in part through its interaction with NRF2 [18,19]. Specifically, phosphorylation of NRF2 by GSK3 β promotes its removal from the nucleus, thereby attenuating NRF2-mediated transcription [20].

The GSK3 β -NRF2 is a key pathway regulating cellular redox homeostasis. In this pathway, activated GSK3 β promotes ubiquitination and subsequent degradation of NRF2, whereas inhibition of GSK3 β facilitates NRF2 activation, thereby inducing the upregulation of antioxidant genes to counteract oxidative stress [21,22]. Although the interaction between GSK3 β and NRF2 has been well established, whether this dual regulatory mechanism influences CKD progression and therapeutic approaches remain to be clarified.

Ligustroflavone (LIG), a flavonoid compound extracted from *Ligustrum lucidum* [23,24], exhibits multiple biological and pharmacological activities. It has been reported to possess anti-inflammatory, antioxidant, and anti-fibrotic properties [25,26]. The fruit of *Ligustrum lucidum* (*Fructus Ligustri Lucidi*, FLL) is a commonly used traditional herbal medicine for treating endocrine and kidney diseases and for strengthening bones [27,28]. Clinical studies have further shown that FLL can mitigate liver and neural injury by modulating oxidative stress-related pathways [26,29]. In this study, we investigated the potential anti-fibrotic and anti-inflammatory effects of ligustroflavone in CKD and explored its underlying mechanisms.

Methods

Animal breeding, ligustroflavone treatment, and construction of CKD mouse models

Male C57BL/6J mice (8 weeks old, approximately 25 g) were purchased from the Experimental Animal Center of Nanjing Medical University. All animals were housed under controlled laboratory conditions with free access to food and water. The UUO model was established using standard surgical procedures to induce CKD [30]. After a minimum 7-day acclimatization period, mice were randomly divided into four groups ($n = 6$ per group): sham-operation group, UUO group, LIG + sham group, and LIG + UUO group. In the UUO group, mice underwent unilateral ureter ligation to induce CKD. Ligustroflavone (Purity: 99.9%; T3802, Targetmol, china) was administered at 30 mg/kg body weight by daily intragastric gavage, following previously reported protocols [26]. Mice received either vehicle (10% DMSO+40% PEG300 + 5% Tween-80 + 45% saline, v/v) or a 30 mg/kg ligustroflavone (dissolved in vehicle) solution once daily for 7 days after surgery. In folic acid-induced nephropathy (FAN) mouse model, mice were randomly divided into four groups ($n = 6$ per group): Vehicle group, Vehicle + FAN group, LIG group, and LIG + FAN group. In the FAN group, mice were intraperitoneal (i.p) injection with 250 mg/kg folic acid (F7876, Sigma-Aldrich, USA) dissolved in 0.3 M sodium bicarbonate (vehicle) as previously described [31]. Control animals received equal volume of vehicle (i.p). Mice were sacrificed after 15 days of FA administration. At the end of the experiment, blood collection from inferior vena cava under anesthesia, then the mice were euthanized through cervical dislocation and kidney tissues were collected and preserved for subsequent analyses. Only male mice were used in this study, as estrogen can influence fibrosis development. All animal procedures were performed in accordance with the guidelines of the Animal Ethics Committee of Nanjing Medical University (approval number: IACUC 2310025-2).

Cell culture

MPTCs (CRL-3361, ATCC, USA) and NRK-49F fibroblasts (CRL-1570, ATCC, USA) were obtained from the American Type Culture Collection (ATCC, Virginia, USA). MPTCs were cultured in DMEM/F-12 medium (11320033, Gibco, USA) supplemented with 10% fetal bovine serum (FBS), 100 µg/mL streptomycin, and 100 µg/mL penicillin, at 37 °C, in a humidified incubator with 5% CO₂. To evaluate the effects of ligustroflavone, MPTCs were exposed to different concentrations of ligustroflavone for 24 h. For ferroptosis induction, MPTCs were pre-treated with 20 µM ligustroflavone for 1 h, followed by exposure to erastin (10 µM, 571203-78-6, MCE, China) for 24 h. The culture supernatant from MPTCs treated with ligustroflavone and erastin was subsequently applied to NRK-49F cells for co-culture experiments. For gene silencing, mouse GSK3β CRISPR/Cas9 plasmids (sequence provided in Supplementary Table 1) were purchased from Tsingke Biotechnology (Nanjing, China). MPTCs were transfected with either an empty vector or GSK3β-knockout plasmids using Lipofectamine 2000 (11668030, Thermo Fisher Scientific, USA). Cells were harvested for subsequent analyses.

Quantitative real-time reverse transcription polymerase chain reaction (qRT-PCR) and Western blotting (WB)

Total RNA was extracted from cells or kidney tissues using TRIzol reagent (9108, Takara, Japan). cDNA was synthesized using reverse transcription reagents (2641A, Takara, Japan). qRT-PCR was performed on an ABI system (QuantStudio 3, Applied Biosystems, California, USA) using SYBR Green dye (Q311-02, vazyme, China). Relative mRNA expression was calculated using the cycle threshold value (ΔCt) method, normalized to housekeeping genes. Primer sequences are listed in Supplementary Table 1. For Western blotting, kidney tissue, MPTCs, and NRK-49F cells were lysed in RIPA buffer (P0013B, Beyotime, china) supplemented with protease inhibitors (11697498001, Roche, Indianapolis, USA). Equal volumes of protein samples were subjected to SDS-PAGE and transferred to membranes for immunoblotting. Protein bands were visualized using an enhanced chemiluminescence (ECL) system (Bio-Rad, California) and quantified with ImageJ software (National Institutes of Health, USA). Primary and secondary antibodies are listed in Supplementary Table 2.

Sirius Red and PAS (Periodic acid Schiff) staining

Kidney tissues were fixed in 4% paraformaldehyde, embedded in paraffin, and sectioned into 4-micron-thick sections using a microtome. Following deparaffinization and rehydration, sections were stained with Sirius Red (RS1220, G-CLONE, china) or PAS (G1281, Solarbio, china). Fibrotic areas in the renal cortex were assessed in a double-blind manner using Sirius Red staining [32]. Images were acquired using an Olympus microscope (BX51, Tokyo, Japan) at 200× magnification. The renal injury scores (0–4) were analyzed and valued based on the percentage of the histological damage to the renal tissue, characterized by cast formation, tubular cell lysis, dilation, and loss of brush border as described in previous studies [33,34]: 0, no abnormalities; 1+, < 25%; 2+, 25–50%; 3+, 50–75%; and 4+, >75%.

Immunofluorescence (IF) staining

NRK-49F cells were seeded on coverslips, fixed with 10% formaldehyde, and subjected to immunofluorescence staining. Mouse kidney tissues were fixed in formaldehyde and dehydrated. After permeabilization with 0.5% Triton X-100 (ST1723, beyotime, China), nonspecific binding was blocked with FBS. Samples were then incubated sequentially with primary and secondary antibodies. Fluorescence images were captured using a fluorescence microscope (Carl Zeiss, Oberkochen, Germany). Antibodies are listed in Supplementary Table 3.

Immunohistochemical (IHC) staining

Kidney tissue samples were sectioned at 4 µm thickness, deparaffinized, and incubated in citrate buffer for antigen retrieval. Endogenous peroxidase activity was blocked with H₂O₂, followed by blocking with bovine serum albumin (ST2249, beyotime, China). Sections were then incubated with primary and secondary antibodies

(listed in Supplementary Table 3). Immunohistochemical images were captured using a microscope (Olympus Corporation, Tokyo, Japan). Positive staining areas were semi-quantitatively analyzed using ImageJ software.

TUNEL and cell viability assays (TUNEL, CCK-8, LDH, and EdU)

Apoptotic cells in kidney tissue sections were detected using the BrightGreen TUNEL kit (A112-01/02/03, Vazyme, China) according to the manufacturer's instructions. Briefly, the TdT solution was applied to the sections, and apoptotic cells were visualized with a fluorescence microscope (Carl Zeiss, Oberkochen, Germany). For each sample, at least five random fields were imaged at 200× magnification under dark-field conditions, and the number of TUNEL-positive cells was quantified.

Cell viability was measured using the CCK8 kit (C0037, Beyotime, China). CCK-8 reagent was added to cultured MPTCs and incubated in an incubator for 1–4 h, after which absorbance was measured. Cytotoxicity was further evaluated by quantifying lactate dehydrogenase (LDH) release in the culture medium using a biochemical analyzer (Hitachi, Tokyo, Japan).

Proliferation of NRK-49F was assessed with the EdU kit (C0071S, Beyotime, China) according to the manufacturer's protocol. Briefly, the EdU solution was added to cell cultures to incorporate into newly synthesized DNA. Cells were then stained with Apollo Green fluorescent dye to label proliferating cells and counterstained with Hoechst for nuclear visualization. Images were acquired using a fluorescence microscope, and fibroblast proliferation was expressed as the percentage of EdU-positive cells.

Determination of lipid peroxidation

Lipid peroxidation was evaluated using the BODIPY-C11 fluorescent probe (D3861, Thermo Fisher, Massachusetts, USA), which detects lipid peroxidation in living cells. MPTCs were seeded in confocal culture dishes and co-cultured with Erastin and/or ligustroflavone, then stained with BODIPY-C11. Fluorescence at different wavelengths was recorded using a laser confocal microscope. To further assess ferroptosis, glutathione (GSH), glutathione disulfide (GSSG), and malondialdehyde (MDA) levels were quantified, as these are markers of lipid peroxidation. The GSH/GSSG ratio was determined using a commercial kit (S0053, Beyotime, China). MDA levels in kidney tissues and MPTCs samples were measured using a Beyotime kit (S0131S, Beyotime, China). Absorbance values for GSH/GSSG and MDA were analyzed with a microplate reader (Thermo Multiskan FC, Thermofisher, USA).

Determination of iron content

Intracellular and tissue Fe^{2+} levels were measured with an iron assay kit (BC5410, solarbio Biotechnology, China) according to the manufacturer's instructions. Absorbance was read at 520 nm using a microplate reader, and iron levels were expressed as $\mu\text{mol}/\text{mg}$ protein.

Cellular thermal shift assay (CETSA)

To detect the possible direct binding of ligustroflavone to GSK3 β , CETSA assay was performed as previously described [35]. Briefly, mPTCs were treated with 20 μM ligustroflavone or vehicle (DMSO) for 4 h and then suspended in PBS. The suspension was divided into six aliquots (about 10^6 cells/aliquot) and heated individually at different temperatures (42, 44, 46, 48, 50, and 52 °C) for 3 min. Next, the cells were lysed using three freeze–thaw cycles (a protease inhibitor was added). Finally, western blot was performed to detect GSK3 β protein levels in the supernatants.

Statistical analysis

All data are expressed as the mean \pm standard deviation (SD). Normalcy was evaluated for all data sets generated in this study using the unpaired Student's t-test, one-way or two-way ANOVA using GraphPad Prism 6.0 (GraphPad Software, California, USA) and the specific statistical test employed to compare paired or grouped data is added to the figure legend. A p -value < 0.05 was considered statistically significant.

Results

Ligustroflavone reduces renal tubular injury and renal fibrosis in UUO mice

Compared with the sham-operated group, PAS staining revealed that kidneys from UUO mice exhibited marked structural abnormalities, including tubular lumen dilation and brush border detachment (Figure 1(A)). In contrast, ligustroflavone-treated mice displayed significantly lesser tubular and interstitial injury than untreated UUO mice. Extracellular matrix deposition was evaluated using Sirius Red staining to assess renal fibrosis. Collagen accumulation in the renal interstitium was markedly increased in UUO mice, indicating severe fibrosis. However, ligustroflavone treatment significantly reduced matrix deposition (Figure 1(B)). Immunofluorescence analysis of COL1A1 (collagen type I alpha 1) showed negative staining in both sham ligustroflavone-treated groups. In UUO mice, COL1A1 expression was strongly upregulated, whereas ligustroflavone administration significantly suppressed its expression (Figure 1(C)). Similarly, the expression of fibronectin and α -SMA proteins was markedly elevated in UUO renal tissues compared with controls. Ligustroflavone treatment effectively inhibited the upregulation of these fibrosis-related proteins (Figure 1(D)). Additionally, there was no obvious renal, liver, or heart damage after daily gavage with

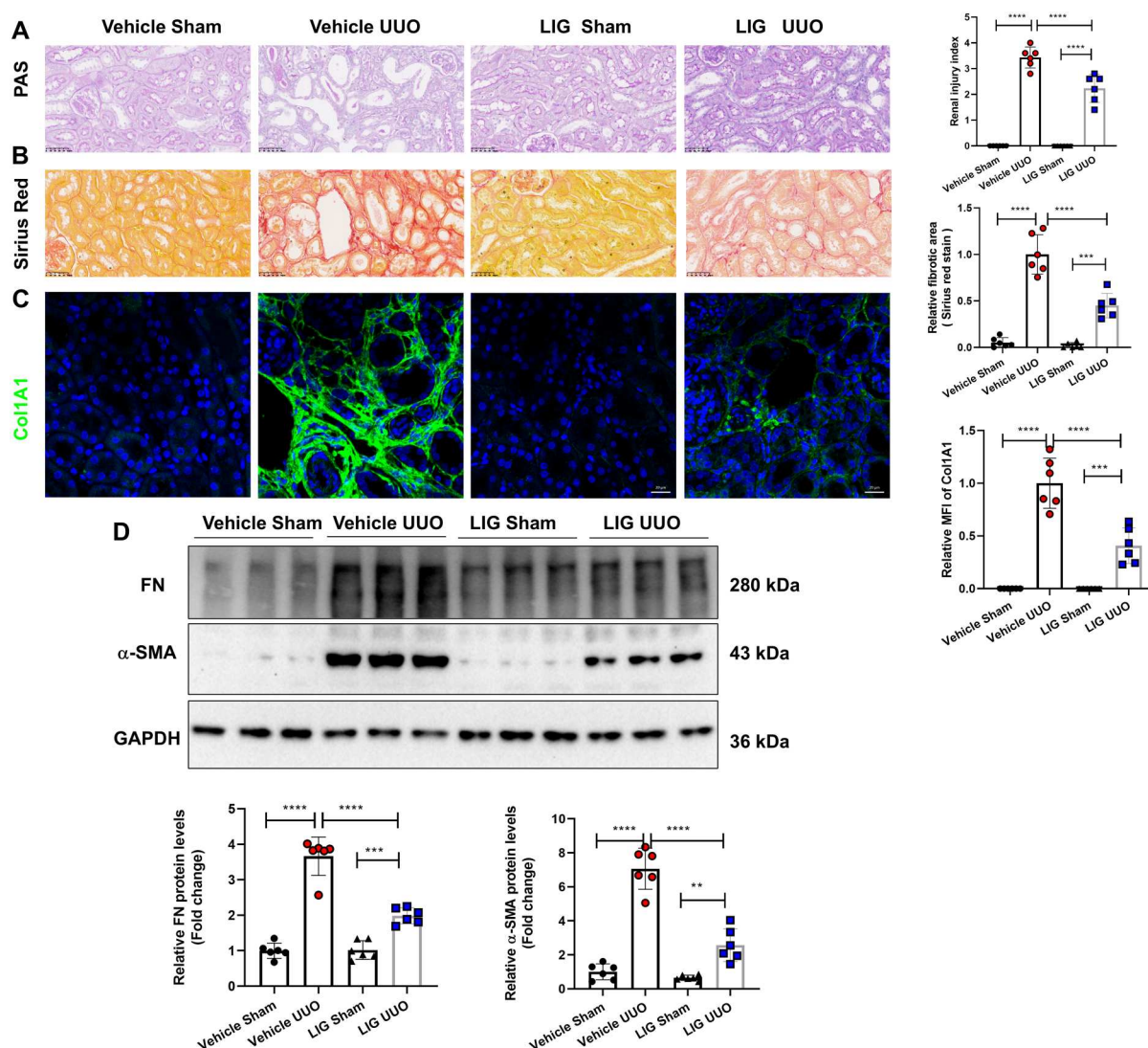


Figure 1. Ligustroflavone improves renal interstitial fibrosis in UUO mice. (A) PAS staining of kidney tissues and tubular injury index; magnification, 400 \times ; scale bar, 20 μ m (B) Sirius Red staining of kidney tissues with semi-quantitative analysis by ImageJ. (C) IHC staining of collagen I with semi-quantitative analysis by ImageJ. (D) Western blot analysis of fibronectin and α -SMA expression in kidney tissues with corresponding densitometric quantification. Data are presented as mean \pm S.D. (n = 6). **** P < 0.0001, *** P < 0.001, ** P < 0.01. (One-way ANOVA).

ligustroflavone for 21 days, compared with control group, suggesting no visible toxic effects of ligustroflavone in the mice (Supplementary Figure 1). Together, these findings indicate that ligustroflavone attenuates renal tubular injury and fibrosis induced by UUO.

Ligustroflavone improves the inflammation and death of RTECs caused by ureteral obstruction

Inflammatory responses and RTECs death are important mechanisms of early CKD injury. TUNEL staining revealed a marked increase in RTECs apoptosis in UUO kidneys compared with sham-operated controls, whereas ligustroflavone administration significantly reduced RTECs death (Figure 2(A)).

Western blot analysis (Figure 2(B)) further demonstrated that ligustroflavone treatment reversed the UUO-induced upregulation of KIM-1 and NGAL, established markers of renal tubular injury.

Inflammation is a hallmark of tubular damage in CKD, characterized by infiltration of immune cells and production of proinflammatory cytokines. IHC staining showed that F4/80-positive macrophages were significantly increased in UUO kidneys compared with sham controls. Ligustroflavone treatment markedly

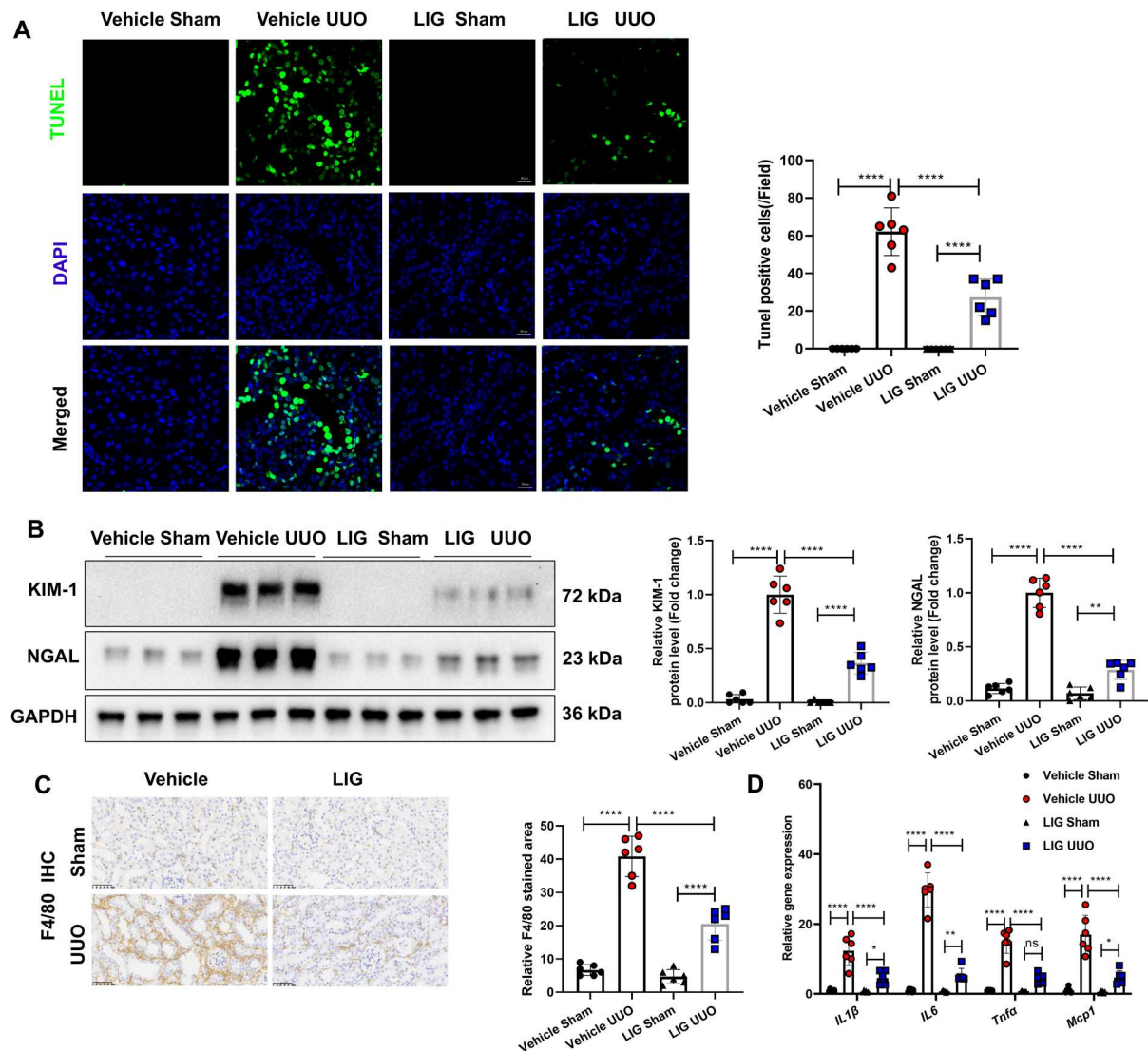


Figure 2. Ligustroflavone attenuates inflammation and death of RTECs caused by UUO. (A) TUNEL staining of renal tissues (magnification 400×; scale bar, 20 μm; green: TUNEL; blue: DAPI). Semi-quantitative analysis of TUNEL-positive cells is shown. (B) Western blot analysis of KIM-1 and NGAL protein expression in renal tissues. Band densities were quantified using ImageJ, with statistical results shown to the right. (C) IHC staining of F4/80 in renal tissues (magnification, 400×; scale bar, 20 μm), Semi-quantitative analysis by ImageJ is shown to the right. (D) Expression of IL1β, IL6, TNFα, and MCP1 genes in renal tissues measured by qRT-PCR. Data are presented as mean ± SD (n = 6). **** $P < 0.0001$, *** $P < 0.001$, ** $P < 0.01$, * $P < 0.05$ (one-way ANOVA for A, B, C, two-way ANOVA for D).

reduced macrophage infiltration (Figure 2(C)). Consistent with these findings, qRT-PCR analysis demonstrated that ligustroflavone significantly decreased expression of pro-inflammatory cytokines, including IL1 β , IL6, TNF α , and MCP1, in UUO kidneys (Figure 2(D)). Together, these results indicate that ligustroflavone protects RTECs from UUO-induced apoptosis and suppresses inflammatory cell infiltration and cytokine production.

Ligustroflavone activated the GSK3 β /NRF2 pathway

Previous studies have shown that ligustroflavone has antioxidant properties [29], but its precise mechanism of action remains unclear. To explore the molecular mechanism underlying its protective effects in CKD, we predicted potential ligustroflavone targets using SwisstargetPrediction software. Candidate targets were further analyzed by molecular docking with AutoDock (version 4.2.6). Docking results indicated that ligustroflavone could directly bind to GSK3 β , which mediates NRF2 phosphorylation and degradation (Figure 3(A,B)). A CCK-8 assay demonstrated that ligustroflavone (10-200 μ mol/l) had no cytotoxic effects on MPTCs compared with vehicle. However, at 200 μ mol/l, ligustroflavone significantly reduced MPTC viability

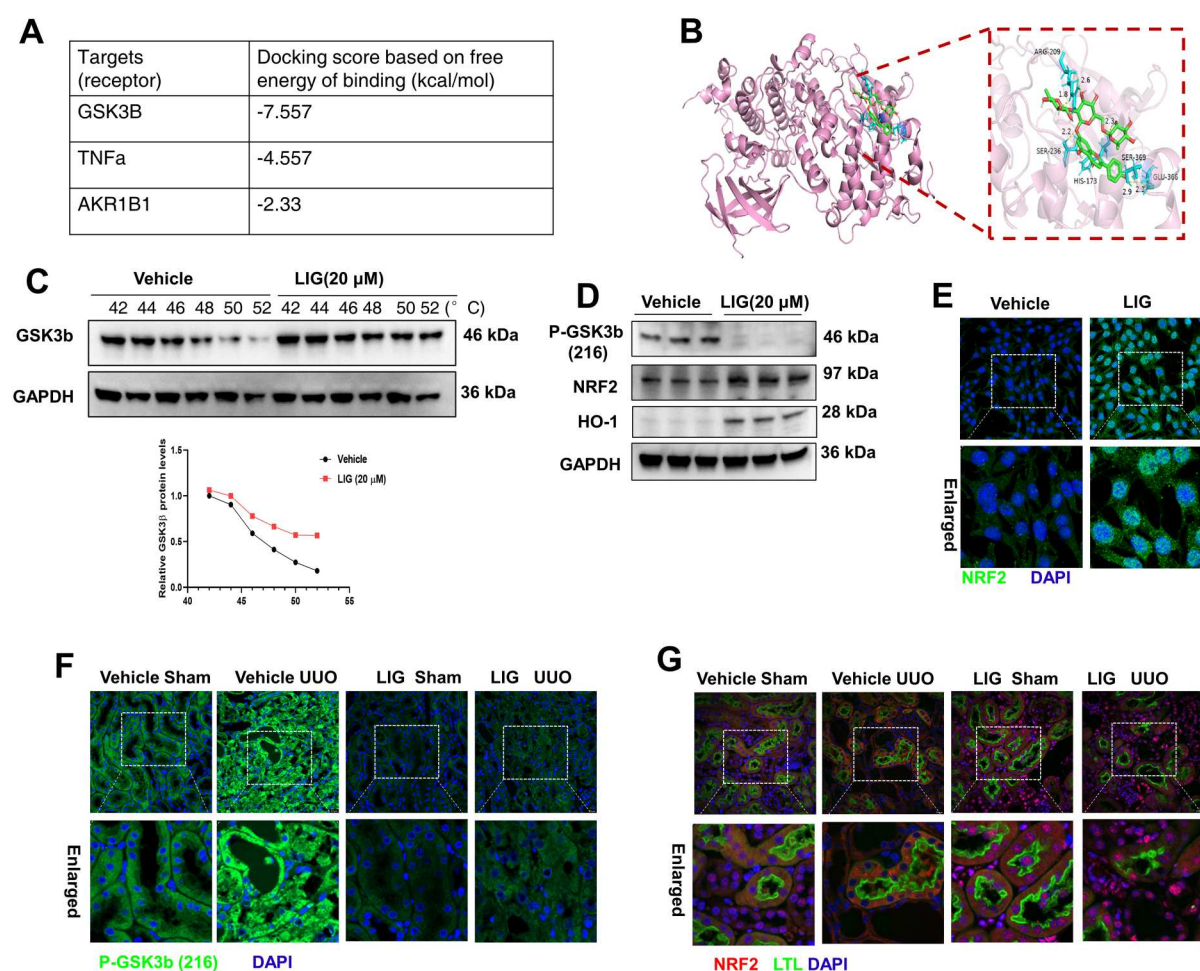


Figure 3. Ligustroflavone acting on the GSK3 β /NRF2 pathway. (A, B) Predicted interaction between ligustroflavone and GSK3 β using target prediction and molecular docking software. (C) Cellular thermal shift assay (CETSA) of GSK3 β with or without ligustroflavone (20 μ mol/L) in MPTCs, band densities were quantified using ImageJ, the below image is the statistical results. (D) Western blot analysis of phosphorylated GSK3 β (p-GSK3 β), NRF2, and HO-1 in MPTCs with or without ligustroflavone (20 μ M) pretreatment. (E) Immunofluorescence analysis of NRF2 nuclear localization in MPTCs treated with ligustroflavone (20 μ mol/L). Quantification was performed using ImageJ. (F) Immunofluorescence analysis of p-GSK3 β nuclear co-localization. (G) Immunofluorescence analysis of NRF2 and Lotus tetragonolobus lectin (LTL) co-localization in renal tissues after 7 days of intragastric ligustroflavone (30 mg/kg) treatment with or without UUO. Data are presented as mean \pm SD (n = 6). **** P < 0.0001, *** P < 0.001, ** P < 0.01. (One-way ANOVA).

relative to lower concentrations (Supplementary Figure 1A). Additionally, CETSA assay was used to analyze the direct binding of ligustroflavone to GSK3 β . The results showed that ligustroflavone treatment induced a right shift in the thermal melting curve of GSK3 β (Figure 3(C)). When MPTCs were treated with ligustroflavone (20 μ M) for 24 h, phosphorylation of GSK3 β at Tyr216 was significantly reduced, indicating GSK3 β inhibition. Concurrently, NRF2 and HO-1 expression levels were upregulated (Figure 3(D) & Supplementary Figure 2C), with the mRNA levels of GSK3 β were not affect (Supplementary Figure 2B). Immunofluorescence analysis further confirmed that ligustroflavone enhanced NRF2 nuclear localization (Figure 3(E) & Supplementary Figure 2D). In vivo, oral administration of ligustroflavone (30 mg/kg) for 7 days effectively inhibited GSK3 β activity in renal tissues (Figure 3(F) & Supplementary Figure 2E). Fluorescence imaging demonstrated co-localization of Lotus tetragonolobus lectin (LTL, a marker of proximal tubules) with NRF2 following treatment (Figure 3(G) & Supplementary Figure 2F). However, the mRNA levels of GSK3 β were not affect after ligustroflavone treatment (Supplementary Figure 2G). Collectively, these results indicate that ligustroflavone suppresses GSK3 β activity and promotes NRF2 activation in renal tubules.

Ligustroflavone prevents ferroptosis in renal tubular interstitium caused by UO

NRF2 plays a critical role in GPX4-dependent ferroptosis [36,37]. Therefore, we investigated whether ligustroflavone protects against ferroptosis by regulating the NRF2/GPX4 axis. Chelatable Fe²⁺ content in kidney tissues was first measured. Compared with control mice, Fe²⁺ levels were significantly elevated in UO kidneys, whereas ligustroflavone treatment reduced Fe²⁺ accumulation (Figure 4(A)). UO also decreased the GSH/GSSG ratio in kidney tissues, while ligustroflavone treatment significantly restored this ratio (Figure 4(B)). Similarly, ligustroflavone reduced UO-induced increase in MDA levels (Figure 4(C)). Long-chain acyl-CoA synthetase 4 (ACSL4) is a key driver of ferroptosis, whereas prostaglandin-endoperoxide synthase 2 (PTGS2) is considered a downstream marker of lipid peroxidation and inflammation. qRT-PCR revealed that ACSL4 and PTGS2 mRNA expression was significantly increased in UO kidneys compared with controls (Figure 4(D)). Western blot analysis demonstrated that ligustroflavone reduced UO-induced p-GSK3 β expression while upregulating NRF2 and GPX4 protein levels (Figure 4(E)). To assess lipid peroxidation, 4-hydroxynonenal (4-HNE), a major end-product of lipid peroxidation and biomarker of oxidative stress, was examined by IHC. UO markedly increased 4-HNE expression, whereas ligustroflavone treatment restored normal levels (Figure 4(F)).

Finally, mitochondrial ultrastructure was evaluated by transmission electron microscopy (TEM). Control kidneys displayed normal mitochondria, whereas UO kidneys exhibited severe structural damage, including cristae disintegration, atrophy, and membrane rupture. Remarkably, ligustroflavone treatment alleviated mitochondrial injury (Figure 4(G)).

Ligustroflavone prevents ferroptosis in MPTCs via the GSK3 β pathway

Erastin is a widely used inducer of ferroptosis[38]. Cell viability assays showed that ligustroflavone attenuated Erastin-induced cytotoxicity in MPTCs in a concentration-dependent manner, with maximal protective effects observed at 20 μ M (Figure 5(A)).

At this concentration, ligustroflavone reduced Erastin-induced lactate dehydrogenase (LDH) release and MDA accumulation (Figure 5(B and C)). Erastin also decreased the GSH/GSSG ratio in MPTCs, whereas ligustroflavone treatment restored this ratio (Figure 5(D)). BODIPY-C11 staining was used to assess lipid peroxidation. Erastin caused a shift in the BODIPY-C11 fluorescence from red (reduced state) to green (oxidized state). Ligustroflavone treatment reversed this shift, restoring predominantly red fluorescence, consistent with reduced lipid peroxidation (Figure 5(E)).

To determine whether the protective effect of ligustroflavone against ferroptosis is mediated by GSK3 β , GSK3 β was silenced in MPTCs (Figure 5(F)). Ligustroflavone improved cell viability in Erastin-treated MPTCs in the negative control (NC) group. However, in the GSK3 β knockout (KO) group, ligustroflavone failed to rescue cell viability (Figure 5(G)). These findings indicate that ligustroflavone exerts its anti-ferroptotic effects in MPTCs through activation of the GSK3 β pathway.

To evaluate whether ligustroflavone affects renal myofibroblast activation, NRK-49F cells were cultured with supernatants from MPTCs pretreated with Erastin (10 μ M) and/or ligustroflavone (20 μ M). EdU assays

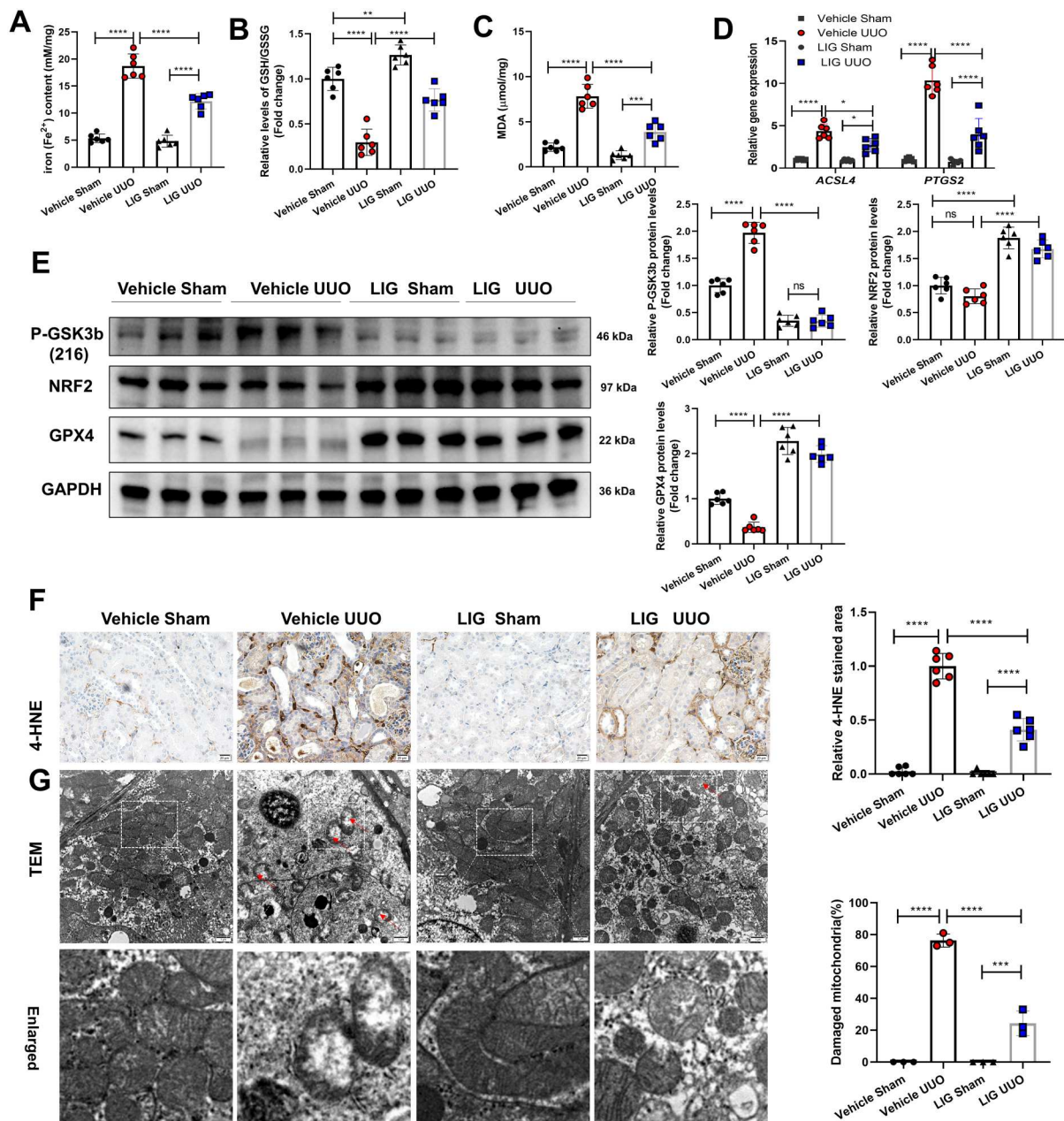


Figure 4. Ligustroflavone prevents ferroptosis in UUO mice. (A) Iron (Fe^{2+}) content in kidney tissues was measured by an assay kit. (B) qRT-PCR analysis of IL1 β , IL6, TNF α and MCP-1 mRNA expression in renal tissues. GSH/GSSG ratio was also measured by qRT-PCR in UUO mice with or without ligustroflavone treatment. (C) MDA levels are measured by an assay kit. (D) qRT-PCR analysis of ACSL4 and PTGS2 expression in UUO kidneys with or without ligustroflavone treatment. (E) Western blot analysis of p-GSK3 β , NRF2, and GPX4 protein expression in UUO kidneys. Band densities were quantified using ImageJ, with statistical results shown to the right. (F) IHC staining of 4-HNE in renal tissues. (G) TEM images of mitochondrial morphology in renal tissues, the red arrow indicated the damaged mitochondria characterized by fracture and absence of mitochondrial cristae (Scale bar, 1 μm). Data are presented as mean \pm SD ($n = 6$). **** $P < 0.0001$, *** $P < 0.001$, ** $P < 0.01$. ns: not significant, (two-way ANOVA for D, one-way ANOVA for other cases).

revealed that supernatant from Erasin-treated MPTCs promoted NRK-49F proliferation, whereas supernatant from MPTCs co-treated with ligustroflavone and Erastin significantly reduced EdU-positive cells. (Figure 6(A)). Immunofluorescence staining demonstrated that Erastin increased α -SMA expression in NRK-49F cells, while ligustroflavone treatment attenuated this increase (Figure 6(B)). These findings suggest that ligustroflavone inhibits NRK-49F activation by suppressing ferroptosis in MPTCs.

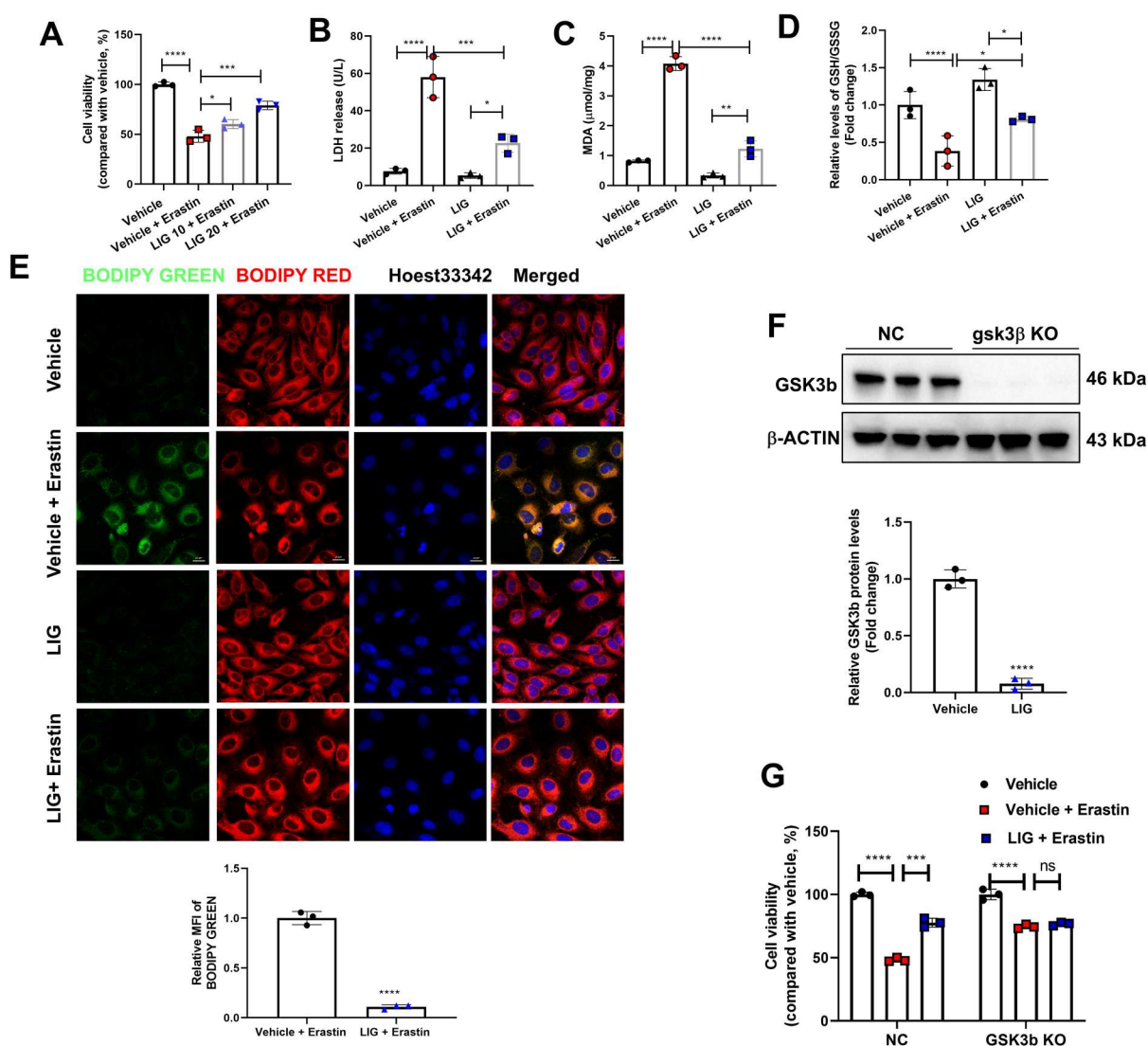


Figure 5. Ligustroflavone prevents ferroptosis in MPTCs via the GSK3 β pathway. (A) CCK8 assay of MPTC viability. (B) LDH release in MPTCs was measured by a biochemical analyzer. (C) MDA levels in MPTCs were measured by an assay kit. (D) GSH/GSSG ratio in MPTCs by assay kit. (E) Immunofluorescence staining of MPTCs with BODIPY-C11 probe (scale bar, 10 μ m; green: oxidized lipids; red: reduced lipids; blue: Hoechst). Semi-quantitative ImageJ analysis shown below. (F) Western blot analysis of GSK3 β protein expression in MPTCs. Band densities were quantified by ImageJ with statistical results shown below. (G) Cell viability was measured by CCK-8 assay, compared between control and GSK3 β knockout models. Data are presented as mean \pm SD (n = 6). **** P < 0.0001, *** P < 0.001, * P < 0.05, ns: no statistical difference (one-way ANOVA).

ligustroflavone attenuated progression of CKD in a FAN mouse model

Folic acid-induced nephropathy (FAN) mouse model is another stable and well-established model used to investigate the pathogenesis of CKD. We found that ligustroflavone greatly mitigated collagens deposition around renal tubules caused by FAN (Figure 7(A)). Ligustroflavone substantially reduced the expression of fibronectin and α -SMA, which were strongly induced in the FAN group (Figure 7(B)). This observation proved that ligustroflavone decreased kidney fibrosis and ameliorated ferroptosis-associated injury in FAN-induced CKD.

Discussion

CKD is characterized by an extremely complex pathological process in which multiple harmful factors impair renal structure and function. Persistent chronic inflammation initiates fibrosis, activates renal interstitial cells,

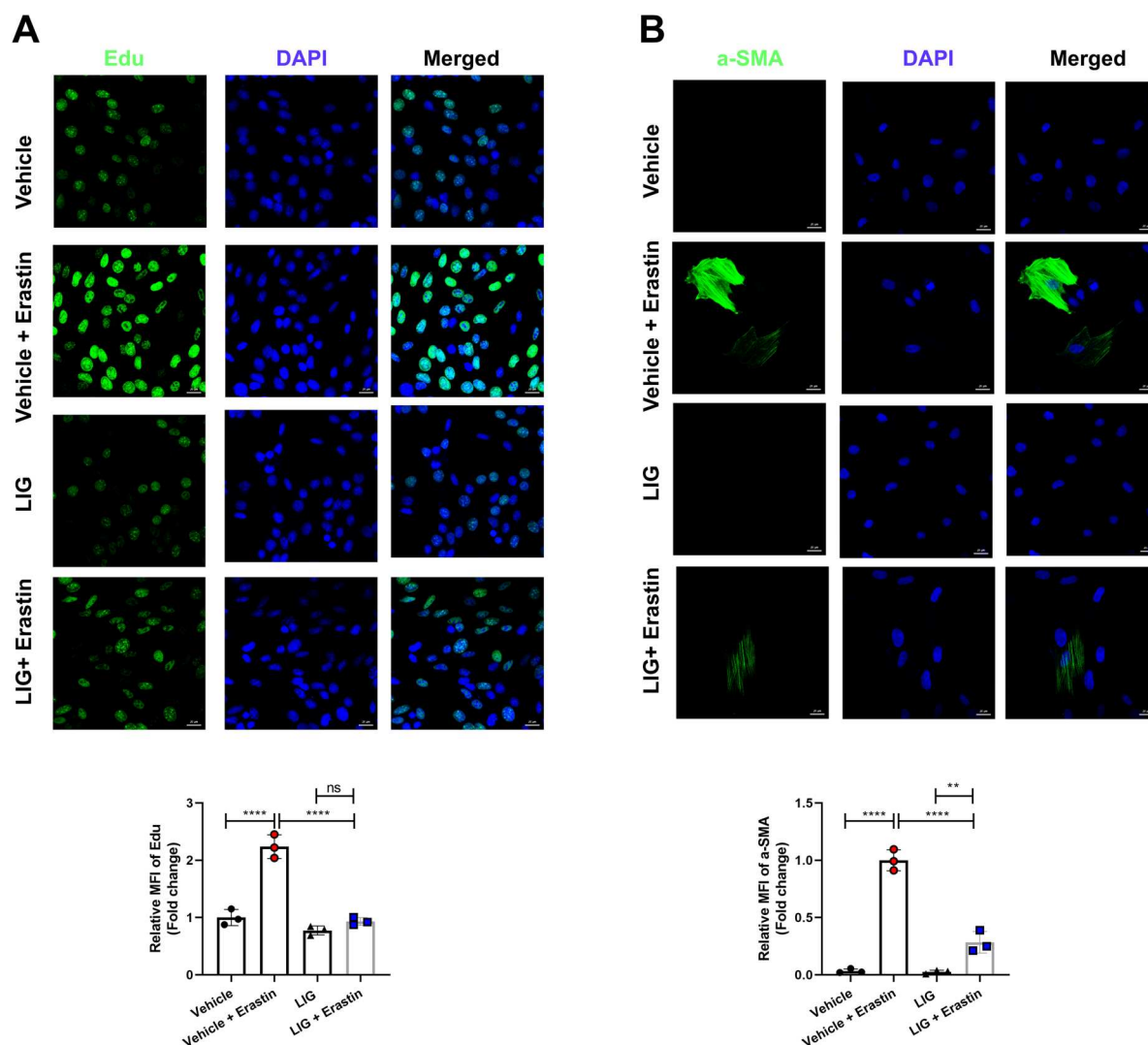


Figure 6. Supernatant from ligustroflavone-pretreated MPTCs inhibits NRK-49F activation. (A) EdU assay of NRK-49F proliferation. Semi-quantitative ImageJ analysis shown below (scale bar, 20 μ m). (B) Immunofluorescence staining of α -SMA expression in NRK-49F cells. Semi-quantitative ImageJ analysis shown below. (scale bar, 20 μ m). Data are presented as mean \pm SD ($n = 6$). **** $P < 0.0001$, ** $P < 0.01$ ns: no statistical difference (one-way ANOVA).

promotes the expression of fibrosis-related cytokines, and increases extracellular matrix (ECM) deposition, including fibrin and collagen, ultimately leading to renal fibrosis [39]. Because no effective strategy currently exists to reverse or halt CKD progression, the development of novel targeted therapies is urgently needed. In this study, using both cell and animal models, we investigated the renoprotective effects against ferroptosis in CKD, representing the first report of its role in this context.

Ligustri Lucidi Fructus (LLF), derived from the dried mature fruits of *Ligustrum lucidum* Ait (Oleaceae), is a widely used traditional Chinese medicinal material [40]. Ligustroflavone, a characteristic flavonoid isolated from LLF, is one of its key bioactive ingredients. Previous studies have demonstrated that ligustroflavone possesses antioxidant [41], anti-tumor [42], and anti-osteoporosis properties [43]. Additional pharmacological activities include anti-inflammatory [23] and anti-complement effects [24]. Moreover, ligustroflavone acts as an antagonist of the calcium-sensing receptor, a mechanism that contributes to its anti-osteoporosis effects in diabetes [41]. It has also been shown to reduce necroptosis in rat brains following ischemic stroke by targeting the RIPK1/RIPK3/MLKL pathway [25].

Our findings expand on these pharmacological properties by demonstrating that ligustroflavone protects against kidney injury. In the CKD mouse model induced by UUO and FAN, ligustroflavone treatment reduced expression of fibrosis markers, including collagen Ia1, fibronectin, and α -SMA, and decreased tubular

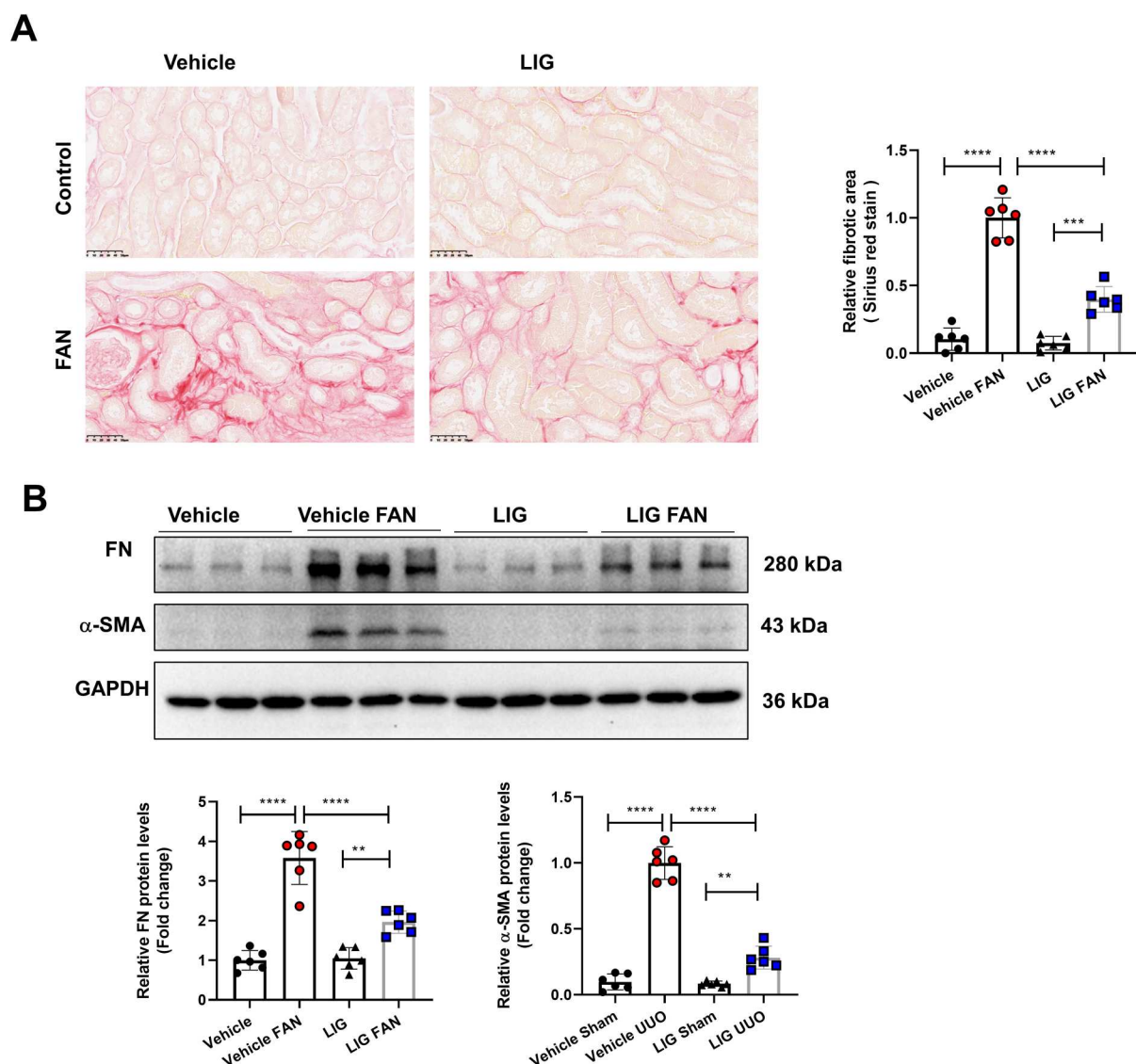


Figure 7. Ligustroflavone improves renal interstitial fibrosis in FAN mice. (A) Sirius Red staining of kidney tissues with semi-quantitative analysis by ImageJ. (B) Western blot analysis of fibronectin and α -SMA expression in kidney tissues with corresponding densitometric quantification. Data are presented as mean \pm S.D. ($n = 6$). **** $P < 0.0001$, *** $P < 0.001$, ** $P < 0.01$. (One-way ANOVA).

apoptosis (TUNEL staining), tubular injury markers (KIM-1 and NGAL), and macrophage infiltration (F4/80). Ligustroflavone also reduced ECM deposition, lipid peroxidation, and interstitial inflammation. Collectively, these results suggest that ligustroflavone is a promising therapeutic candidate for CKD.

Previous studies have demonstrated that ligustroflavone has antioxidant effects [29], but its precise molecular mechanisms remain unclear. To investigate potential mechanisms, we used AutoDock to identify small molecules with stable binding affinity for ligustroflavone. Computational screening predicted that ligustroflavone could bind stably to GSK3 β , potentially triggering downstream biological effects. Notably, GSK3 β mediates ubiquitination and degradation of NRF2. Following ligustroflavone treatment, phosphorylation of GSK3 β at Tyr216 decreased, indicating inhibition of GSK3 β activity, whereas NRF2 and HO-1 expression levels increased. Ligustroflavone also promoted Nrf2 stabilization and nuclear translocation. These findings suggest that the GSK3 β /NRF2/HO-1 pathway is an important mechanism through which ligustroflavone exerts its protective effects.

Progressive CKD is a multifactorial disease with complex pathogenesis involving mitochondrial dysfunction, oxidative stress, chronic inflammation, apoptosis, necrosis, and fibrosis, all of which represent potential

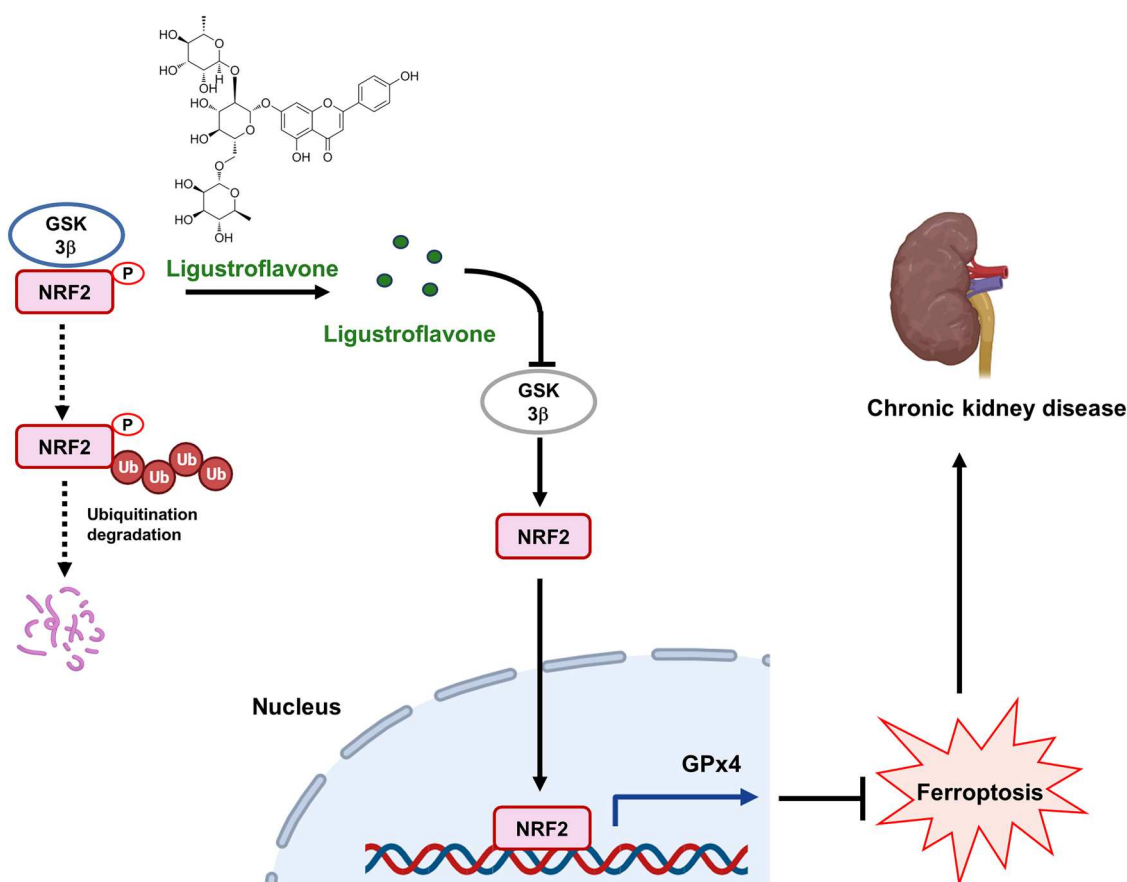


Figure 8. Schematic diagram of our study. Overview of the role and mechanism of ligustroflavone in CKD.

therapeutic targets [4,5]. Recent studies indicate that ferroptosis contributes to several pathogenic processes underlying progressive CKD [44,45]. As noted earlier, NRF2 plays a critical role in GPX4-dependent ferroptosis [36,37]. Accumulating evidence suggests that inhibiting ferroptosis and associated oxidative stress is crucial for alleviating kidney injury. Indeed, in the UUO mouse model, ferroptosis contributes to pathological RTECs death [46]. In our study, ligustroflavone treatment reduced ferroptosis-related alterations, including increased chelatable Fe^{2+} , reduced GSSG/GSH ratio, elevated MDA levels, and upregulation of ACSL4 and PTGS2. Furthermore, ligustroflavone suppressed P-GSK3 β and increased NRF2 and GPX4 expression, while also reducing 4-HNE levels. Together, these findings indicate that ligustroflavone mitigates ferroptosis in UUO kidneys. Ferroptosis is a regulated, iron-dependent form of cell death that occurs when lipid peroxides accumulate and core antioxidant defenses fail [7]. Consistent with this, our *in vitro* experiments demonstrated that ligustroflavone restored MPTC viability following Erastin treatment, reduced LDH release and MDA accumulation, and inhibited NRK-49F activation. Taken together, these results suggest that ligustroflavone improves CKD outcomes by inhibiting ferroptosis in renal tubular epithelial cells.

GSK3 β is widely expressed in the kidney, with its highest enrichment and functional importance in renal tubular epithelial cells (particularly proximal tubules), followed by podocytes and mesangial cells in the glomeruli [47]. Previous studies have reported that GSK3 β may represent an effective therapeutic target for preventing TEC fibrosis and mitigating renal fibrosis [48]. TDZD-8 (a known GSK3b inhibitor) treatment had been found could reduce renal injury and fibrosis in CKD animal models [22]. However, there without GSK3b inhibitors have been used in clinical treatment of CKD. In this study, we demonstrated that ligustroflavone may act as a possible inhibitor of GSK3b to reduce renal injury and fibrosis. Ligustroflavone with clinical translational prospects as it is derived from known plant drugs.

A key question is whether ligustroflavone inhibits ferroptosis in tubular cells induced by Erastin via GSK3 β activation. In our experiments, ligustroflavone treatment restored the GSH/GSSG ratio and reduced lipid peroxidation, as measured by BODIPY-C11 staining, consistent with ferroptosis inhibition. Molecular docking

further suggested that ligustroflavone directly binds to GSK3 β , promoting NRF2 nuclear translocation and enhancing expression of downstream target genes. Interestingly, ligustroflavone treatment also increased GPX4 protein levels in UUO kidneys. These findings support the hypothesis that ligustroflavone exerts its renoprotective effect by modulating the GSK3 β /NRF2 signaling axis, thereby suppressing lipid peroxidation, oxygen metabolism, and alleviating ferroptosis in CKD. However, our study has limitations. We did not confirm a direct physical interaction between ligustroflavone and GSK3 β , although our data suggest that ligustroflavone prevents NRF2 degradation mediated by GSK3 β -dependent ubiquitination. Additional experimental evidence is required to validate the interaction between ligustroflavone and GSK3 β and determine whether ligustroflavone may also act through protective pathways in the kidney.

Conclusion

In summary, our findings suggest that ligustroflavone protects against UUO and FAN-induced CKD by inhibiting ferroptosis and reducing lipid peroxidation via regulation of the GSK3 β /NRF2 pathway (Figure 8). This study confirms both the efficacy and molecular mechanisms of ligustroflavone in renal injury at cellular and animal levels and highlights its potential as a promising therapeutic agent for CKD.

Acknowledgements

Wen Zhang: Data Curation, Formal analysis, Investigation, Project administration, Writing – Original Draft. Shaofan Wang: Data Curation, Formal analysis, Investigation, Project administration, Writing – Original Draft. Yaru Wang: Data Curation, Formal analysis, Methodology, Project administration, Software. Sutianyi Li: Data Curation, Formal analysis, Visualization. Mingyue Chen: Data Curation, Visualization. Jiayu Song: Conceptualization, Funding acquisition, Project administration, Supervision, Validation. Yunwen Yang: Conceptualization, Funding acquisition, Project administration, Supervision, Validation, Resources, Writing – review & editing. All the authors have read and approved the final manuscript.

Author contributions

CRedit: **Wen Zhang:** Data curation, Formal analysis, Investigation, Project administration, Writing – original draft; **Shaofan Wang:** Data curation, Formal analysis, Investigation, Project administration, Writing – original draft; **Yaru Wang:** Data curation, Formal analysis, Methodology, Project administration, Software; **Sutianyi Li:** Data curation, Formal analysis, Visualization; **Mingyue Chen:** Data curation, Visualization; **Jiayu Song:** Conceptualization, Funding acquisition, Project administration, Supervision, Validation; **Yunwen Yang:** Conceptualization, Funding acquisition, Project administration, Resources, Supervision, Validation, Writing – review & editing.

Disclosure statement

No potential conflict of interest was reported by the author(s).

Funding

This study was supported by the National Natural Science Foundation of China (grant number 82370683, 82400816), the Natural Science Foundation of Jiangsu Province (grant number BK20241731), Nanjing Health Science and Technology Development Foundation (grant number ZKX22049), Nanjing Medical University Undergraduate Innovation Training Program Project (grant number X2025103120062) and the Youth Science and Technology Talent Support Program of Jiangsu Province (grant number JSTJ-2025-121).

Data availability statement

The datasets used and/or analyzed during the present study appear in the submitted article.

Ethics statement

All animal procedures were performed in accordance with the guidelines of the Animal Ethics Committee of Nanjing Medical University (approval number: IACUC 2310025-2).

ORCID

Yunwen Yang  <http://orcid.org/0000-0002-1916-5716>

References

- [1] Romagnani P, Remuzzi G, Glasscock R, et al. Chronic kidney disease. *Nat Rev Dis Primers*. 2017;3:17088. doi:10.1038/nrdp.2017.88
- [2] Evans M, Lewis RD, Morgan AR, et al. A Narrative Review of Chronic Kidney Disease in Clinical Practice: Current Challenges and Future Perspectives. *Adv Ther*. 2022;39(1):33–43. doi:10.1007/s12325-021-01927-z
- [3] Bennett P, Warren M, Aydin Z, et al. Kidney disease: improving global outcomes (KDIGO) workshop on the Nurse's role in managing the symptoms of people receiving dialysis. *Kidney Int Rep*. 2025;10(2):313–320. doi:10.1016/j.ekir.2024.11.029
- [4] Carney EF. The impact of chronic kidney disease on global health. *Nat Rev Nephrol*. 2020;16(5):251. doi:10.1038/s41581-020-0268-7
- [5] Panizo S, Martinez-Arias L, Alonso-Montes C, et al. Fibrosis in Chronic Kidney disease: Pathogenesis and consequences. *Int J Mol Sci*. 2021;22(1):408 doi:10.3390/ijms22010408
- [6] Djudjaj S, Boor P. Cellular and molecular mechanisms of kidney fibrosis. *Mol Asp Med*. 2019;65:16–36. doi:10.1016/j.mam.2018.06.002
- [7] Dixon SJ, Lemberg KM, Lamprecht MR, et al. Ferroptosis: an iron-dependent form of nonapoptotic cell death. *Cell*. 2012;149(5):1060–1072. doi:10.1016/j.cell.2012.03.042
- [8] Drueke TB, Massy ZA. Vascular calcification in chronic kidney disease: contribution of ferroptosis? *Kidney Int*. 2022;102(6):1209–1211. doi:10.1016/j.kint.2022.08.031
- [9] Wang J, Liu Y, Wang Y, et al. The cross-link between ferroptosis and kidney diseases. *Oxid Med Cell Longevity*. 2021;2021:6654887. doi:10.1155/2021/6654887
- [10] Wang J, Wang Y, Liu Y, et al. Ferroptosis, a new target for treatment of renal injury and fibrosis in a 5/6 nephrectomy-induced CKD rat model. *Cell Death Discov*. 2022;8(1):127. doi:10.1038/s41420-022-00931-8
- [11] Battaglia AM, Chirillo R, Aversa I, et al. Ferroptosis and cancer: mitochondria meet the “Iron Maiden”. *Cells*. 2020;9(6):1505. doi:10.3390/cells9061505
- [12] Abdalkader M, Lampinen R, Kanninen KM, et al. Targeting Nrf2 to Suppress Ferroptosis and Mitochondrial Dysfunction in Neurodegeneration. *Front Neurosci*. 2018;12:466. doi:10.3389/fnins.2018.00466
- [13] Song J, Wang H, Sheng J, et al. Vitexin attenuates chronic kidney disease by inhibiting renal tubular epithelial cell ferroptosis via NRF2 activation. *Mol Med*. 2023;29(1):147. doi:10.1186/s10020-023-00735-1
- [14] He S, Gao Q, Wu X, et al. NAD(+) ameliorates endotoxin-induced acute kidney injury in a sirtuin1-dependent manner via GSK-3beta/Nrf2 signalling pathway. *J Cell Mol Med*. 2022;26(7):1979–1993. doi:10.1111/jcmm.17222
- [15] Grimes CA, Jope RS. The multifaceted roles of glycogen synthase kinase 3beta in cellular signaling. *Prog Neurobiol*. 2001;65(4):391–426. doi:10.1016/S0301-0082(01)00011-9
- [16] Golpich M, Amini E, Hemmati F, et al. Glycogen synthase kinase-3 beta (GSK-3beta) signaling: Implications for Parkinson's disease. *Pharmacol Res*. 2015;97:16–26. doi:10.1016/j.phrs.2015.03.010
- [17] Hooper C, Killick R, Lovestone S. The GSK3 hypothesis of Alzheimer's disease. *J Neurochem*. 2008;104(6):1433–1439. doi:10.1111/j.1471-4159.2007.05194.x
- [18] Rada P, Rojo AI, Chowdhry S, et al. SCF/beta-TrCP promotes glycogen synthase kinase 3-dependent degradation of the Nrf2 transcription factor in a Keap1-independent manner. *Mol Cell Biol*. 2011;31(6):1121–1133. doi:10.1128/MCB.01204-10
- [19] Jain AK, Jaiswal AK. GSK-3beta acts upstream of Fyn kinase in regulation of nuclear export and degradation of NF-E2 related factor 2. *J Biol Chem*. 2007;282(22):16502–16510. doi:10.1074/jbc.M611336200
- [20] Salazar M, Rojo AI, Velasco D, et al. Glycogen synthase kinase-3beta inhibits the xenobiotic and antioxidant cell response by direct phosphorylation and nuclear exclusion of the transcription factor Nrf2. *J Biol Chem*. 2006;281(21):14841–14851. doi:10.1074/jbc.M513737200
- [21] Culbreth M, Aschner M. GSK-3beta, a double-edged sword in Nrf2 regulation: Implications for neurological dysfunction and disease. *F1000Res*. 2018;7:1043. doi:10.12688/f1000research.15239.1
- [22] Jamadar A, Rao R. Glycogen Synthase Kinase-3 Signaling in Acute Kidney Injury. *Nephron*. 2020;144(12):609–612. doi:10.1159/000509354
- [23] Pieroni A, Pachaly P. Isolation and structure elucidation of ligustroflavone, a new apigenin triglycoside from the leaves of *Ligustrum vulgare* L. *Pharmazie*. 2000;55(1):78–80.
- [24] Pieroni A, Pachaly P, Huang Y, et al. Studies on anti-complementary activity of extracts and isolated flavones from *Ligustrum vulgare* and *Phillyrea latifolia* leaves (Oleaceae). *J Ethnopharmacol*. 2000;70(3):213–217. doi:10.1016/S0378-8741(99)00169-5
- [25] Zhang YY, Liu WN, Li YQ, et al. Ligustroflavone reduces necroptosis in rat brain after ischemic stroke through targeting RIPK1/RIPK3/MLKL pathway. *Naunyn-Schmiedeberg's Arch Pharmacol*. 2019;392(9):1085–1095. doi:10.1007/s00210-019-01656-9

- [26] Bi F, Bai Y, Zhang Y, et al. Ligustroflavone exerts neuroprotective activity through suppression of NLRP1 inflammasome in ischaemic stroke mice. *Exp Ther Med*. 2022;25(1):8. doi:10.3892/etm.2022.11707
- [27] Zhang Y, Dong XL, Leung PC, et al. Fructus ligustri lucidi extract improves calcium balance and modulates the calciotropic hormone level and vitamin D-dependent gene expression in aged ovariectomized rats. *Menopause*. 2008;15(3):558–565. doi:10.1097/gme.0b013e31814fad27
- [28] Siu WS, Wong HL, Lau CP, et al. The effects of an antiosteoporosis herbal formula containing epimedii herba, ligustri lucidi fructus and psoraleae fructus on density and structure of rat long bones under tail-suspension, and its mechanisms of action. *Phytother Res*. 2013;27(4):484–492. doi:10.1002/ptr.4743
- [29] Kang R, Tian W, Cao W, et al. Ligustroflavone ameliorates CCl(4)-induced liver fibrosis through down-regulating the TGF-beta/Smad signaling pathway. *Chin J Nat Med*. 2021;19(3):170–180.
- [30] Kramann R, Menzel S. Mouse Models of Kidney Fibrosis. *Methods Mol Biol*. 2021;2299:323–338. doi:10.1007/978-1-0716-1382-5_22
- [31] Miguel V, Tituana J, Herrero JI, et al. Renal tubule Cpt1a overexpression protects from kidney fibrosis by restoring mitochondrial homeostasis. *J Clin Invest*. 2021;131(5):e140695. doi:10.1172/JCI140695
- [32] Turnberg D, Lewis M, Moss J, et al. Complement activation contributes to both glomerular and tubulointerstitial damage in adriamycin nephropathy in mice. *J Immunol*. 2006;177(6):4094–4102. doi:10.4049/jimmunol.177.6.4094
- [33] Weidemann A, Bernhardt WM, Klanke B, et al. HIF activation protects from acute kidney injury. *J Am Soc Nephrol*. 2008;19(3):486–494. doi:10.1681/ASN.2007040419
- [34] Yang Y, Yu X, Zhang Y, et al. Hypoxia-inducible factor prolyl hydroxylase inhibitor roxadustat (FG-4592) protects against cisplatin-induced acute kidney injury. *Clin Sci*. 2018;132(7):825–838. doi:10.1042/CS20171625
- [35] Wang Y, Tang B, Li H, et al. A small-molecule inhibitor of Keap1-Nrf2 interaction attenuates sepsis by selectively augmenting the antibacterial defence of macrophages at infection sites. *EBioMedicine*. 2023;90:104480. doi:10.1016/j.ebiom.2023.104480
- [36] Dodson M, Castro-Portuguez R, Zhang DD. NRF2 plays a critical role in mitigating lipid peroxidation and ferroptosis. *Redox Biol*. 2019;23:101107. doi:10.1016/j.redox.2019.101107
- [37] Gui J, Wang L, Liu J, et al. Ambient particulate matter exposure induces ferroptosis in hippocampal cells through the GSK3B/Nrf2/GPX4 pathway. *Free Radical Biol Med*. 2024;213:359–370. doi:10.1016/j.freeradbiomed.2024.01.045
- [38] Zhao Y, Li Y, Zhang R, et al. The role of Erastin in ferroptosis and its prospects in cancer therapy. *Onco Targets Ther*. 2020;13:5429–5441. doi:10.2147/OTT.S254995
- [39] Gunawardena S, Dayaratne M, Wijesinghe H, et al. A Systematic Review of Renal Pathology in Chronic Kidney Disease of Uncertain Etiology. *Kidney Int Rep*. 2021;6(6):1711–1728. doi:10.1016/j.ekir.2021.03.898
- [40] Gao L, Li C, Wang Z, et al. Ligustri lucidi fructus as a traditional Chinese medicine: a review of its phytochemistry and pharmacology. *Nat Prod Res*. 2015;29(6):493–510. doi:10.1080/14786419.2014.954114
- [41] Feng R, Ding F, Mi XH, et al. Protective effects of Ligustroflavone, an active compound from Ligustrum lucidum, on diabetes-induced osteoporosis in mice: A potential candidate as calcium-sensing receptor antagonist. *Am J Chin Med*. 2019;47(2):457–476. doi:10.1142/S0192415X1950023X
- [42] Jeong JC, Kim JW, Kwon CH, et al. Fructus ligustri lucidi extracts induce human glioma cell death through regulation of Akt/mTOR pathway in vitro and reduce glioma tumor growth in U87MG xenograft mouse model. *Phytother Res*. 2011;25(3):429–434. doi:10.1002/ptr.3265
- [43] Chen B, Wang L, Li L, et al. Fructus Ligustri Lucidi in Osteoporosis: A Review of its Pharmacology, Phytochemistry, Pharmacokinetics and Safety. *Molecules*. 2017;22(9):1469. doi:10.3390/molecules22091469
- [44] Ruiz-Ortega M, Rayego-Mateos S, Lamas S, et al. Targeting the progression of chronic kidney disease. *Nature Reviews Nephrology*. 2020;16(5):269–288. doi:10.1038/s41581-019-0248-y
- [45] Yuan Q, Tang B, Zhang C. Signaling pathways of chronic kidney diseases, implications for therapeutics. *Signal Transduction and Targeted Therapy*. 2022;7(1):182. doi:10.1038/s41392-022-01036-5
- [46] Yang L, Guo J, Yu N, et al. Tocilizumab mimotope alleviates kidney injury and fibrosis by inhibiting IL-6 signaling and ferroptosis in UUO model. *Life Sci*. 2020;261:118487. doi:10.1016/j.lfs.2020.118487
- [47] Li C, Ge Y, Dworkin L, et al. The beta isoform of GSK3 mediates podocyte autonomous injury in proteinuric glomerulopathy. 2016;239(1):23–35. doi:10.1002/path.4692
- [48] Chen B, Wang P, Liang X, et al. Permissive effect of GSK3beta on profibrogenic plasticity of renal tubular cells in progressive chronic kidney disease. *Cell Death Dis*. 2021;12(5):432. doi:10.1038/s41419-021-03709-5